Carbon-nanotube Nanomotor Driven by Graphene Origami

Kun Cai,[1,*] Sreykeo Sun,[2] Jiao Shi,[2] and Qing-Hua Qin[3,†]

[1] *School of Science, Harbin Institute of Technology, Shenzhen 518055, China*

[2] *College of Water Resources and Architectural Engineering, Northwest A&F University, Yangling 712100, China*

[3] *Department of Engineering, Shenzhen MSU-BIT University, Shenzhen 518172, China*

(Received 12 January 2021; revised 10 March 2021; accepted 7 April 2021; published 11 May 2021)

Experiments have shown that graphene origami (GORI) can be formed by compressing a folio graphene ribbon. In this study, the GORI is introduced to a rotary nanomotor built from a double-walled carbon nanotube. By placing several cantilevered GORI around the long inner tube (rotor) of the nanomotor with their tips toward the rotor, the nonbonding interaction between the tips and the rotor becomes strong when their distance is less than 1 nm. Rotationally symmetrical layout of the GORI tends to induce nonzero unidirectional torque on the rotor. Thereout, the rotor is accelerated to rotate until a stable rotational frequency (SRF) is reached on the condition that the stators (short outer tubes) applying equal but opposite torque on the rotor. The molecular-dynamics simulation approach is adopted to verify the procedure of the proposed rotary nanomotor. Conclusions are drawn for fabrication of the present rotary nanomotor.

DOI: 10.1103/PhysRevApplied.15.054017

I. INTRODUCTION

Nanomotor, as an essential component of a nanomachine, can be treated as a signal source or an output power of a nanosystem to produce a motion [1]. According to the motion style, nanomotors can be classified as translational or linear nanomotors and rotary nanomotors. The sp^2 carbon materials, i.e., graphene [2] and carbon nanotubes (CNTs) [3], have extremely high in-plane and in-shell stiffness and strength [4–7]. Moreover, the interlayer friction between the piled graphene sheets or the multiwalled CNTs is ultralow [8–10]. Hence, graphene and CNTs are useful candidate materials for fabricating dynamic nanodevices, such as nanobearings [8,11,12], nanomotors [13–15], nanosensors [16], nanoresonators [17,18], and nanosprings [19,20]. For example, Barreiro *et al.* [14] built a linear nanomotor in which the short outer tube moves along the negative direction of the temperature gradient on the long inner tube. They also observed the rotation of the outer tube. Wang *et al.* [15] proposed theoretically a CNT-based rotary nanomotor, on which the charged blades are driven to rotate by an external alternating current field. Besides, other methods for actuating the rotation of the rotor in a nanomotor, e.g., laser [21–24] and nanofluid [25–27] were investigated.

In 2014, Cai *et al*. [28] discovered a driving mechanism for a CNT-based rotary nanomotor, which contains a rotor and a stator. They found that if a part of the atoms on the stator are fixed after a period of relaxation in a thermostat, the inner tube will have a stable rotational frequency at the 100-gigahertz level. The mechanism reveals that the rotation is actuated by the collision between the rotor and the stator that have drastic thermal vibration at finite temperature, the system transfers a part of thermal energy from its environment into the rotational kinetic energy. Further, systematic research on the dynamic properties of the rotor in the thermally driven rotary nanomotor was implemented [29,30] and the methods for observing the motion of the rotor were also proposed [31].

Based on the same mechanism, several types of rotary nanomotors were developed. For example, diamond wedges were suggested to drive CNTs to rotate [32]. Shi *et al*. [33] used wedged diamond needles to drive a nanoflake to rotate. Lin and Han [34] suggested a cracked edge in graphene for driving the rotation of a CNT. These models make the thermally driven nanomotor more feasible in experiments and potential application in the future.

In this study, we introduce a graphene origami (GORI) [35–37] to drive the CNT rotor to rotate. The molecular-dynamics simulation approach is adopted to verify the feasibility of the present model. Effects of essential factors, such as the geometry of the GORI and temperature, on the rotation are discussed. Some concluding remarks are drawn for potential application in the design of a rotary nanomotor.

*kuncai99@163.com

†qinghua.qin@smbu.edu.cn

II. MODELS AND METHODS

A. Models

By compressing a folio graphene ribbon, the folded end forms phase transition, i.e., sp^3 bonding appears [36]. After releasing the external load, some of the sp^3 bonds still exist. So, a graphene origami (GORI) can be obtained. Bond topology at the tip of the GORI depends on the pressure applied. For simplicity, here, we form GORI with different initial folding angles (α). In Fig. 1(a), a graphene ribbon with the size of 3.27×1.23 nm^2 is folded symmetrically to form an origami with an angle of α [Fig. 1(b)]. After relaxation, the shape of the origami varies significantly [Fig. 1(c)]. The shape of a relaxed GORI (RGORI) depends on the value of α and becomes asymmetric due to the random velocity field of the atoms in the nanosystem in folding. Even in an experiment, it is impossible to fabricate a graphene origami by compressing a folded ribbon due to two reasons. One is that the small ribbon is initially asymmetric because of the inner atoms (saturated atoms) and edge atoms (saturated or unsaturated atoms), forming a bond topology different from a standard hexagon or honeycomb. The other is that the atoms have thermal vibration at a finite temperature. Unlike a macroribbon, on the nanoscale the graphene ribbon keeps vibrating in the experiment. Hence, the bond topology on both edges of the folded ribbon must be different. In summary, an asymmetric origami is more in line with the actual situation.

In the rotary nanomotor we consider in this work [Fig. 1(d)], a long CNT rotor with a length of approximately 10.08 nm is confined by two short CNT stators with a length of approximately 0.49 nm and their distance of approximately 8.36 nm, and is encircled by

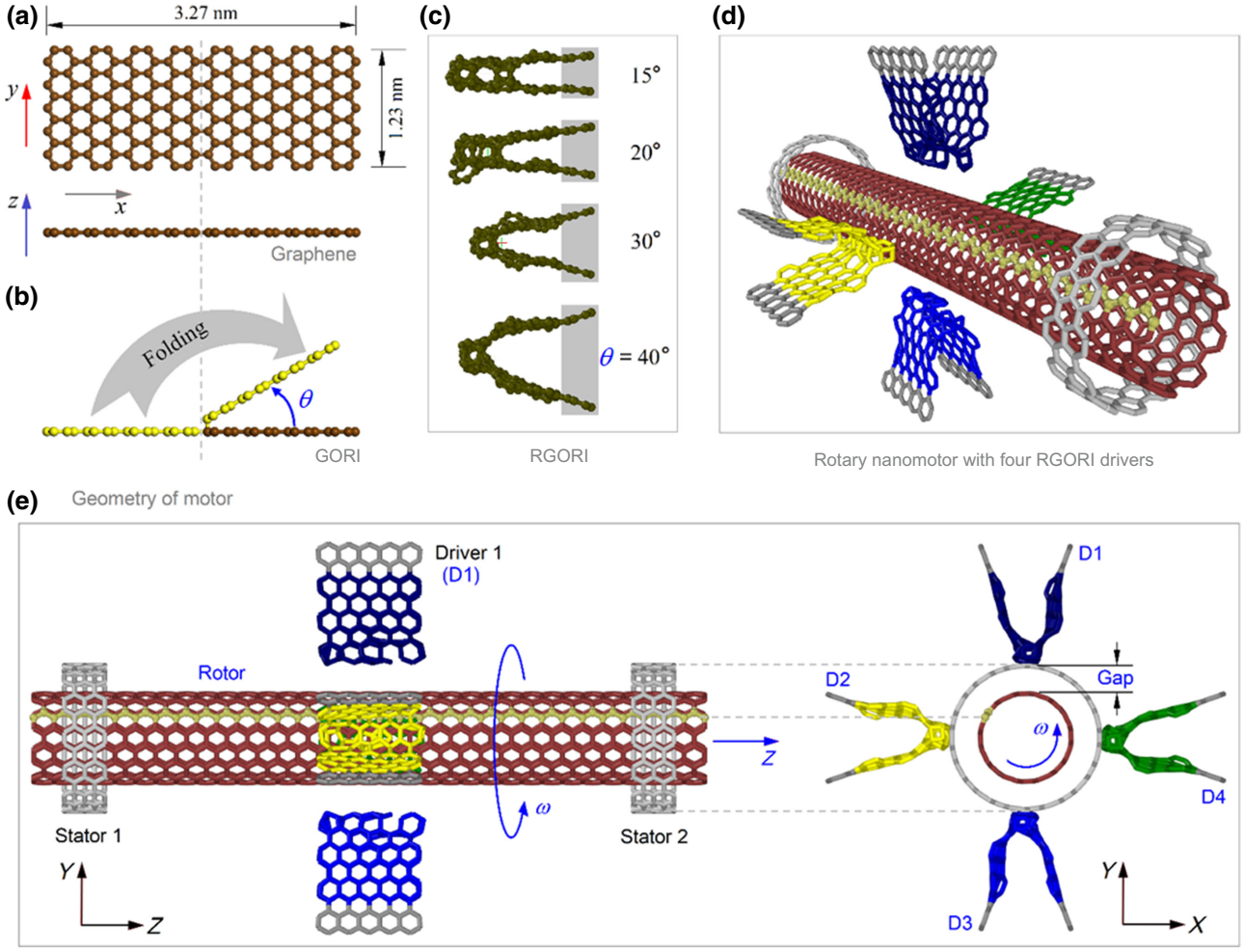

FIG. 1. Rotary nanomotor from CNTs [e.g., with chiral index of (8, 8)/(13, 13)] and GORI. (a) Graphene ribbon with a size of 3.27×1.23 nm^2. (b) Schematic of forming a GORI driver. (c) Configurations of the RGORI with different values of α. In relaxation, the two legs (in the gray area) of each origami are fixed. (d) Perspective of nanomotor. (e) Views of nanomotor consisting of a long CNT rotor, two short CNT stators, and four cantilevered RGORI drivers. "ω" is the rotational frequency of rotor with unit of 1 round/ns (=1 GHz). "Gap" is the distance between the driver's tip and the rotor.

four cantilevered RGORI drivers in rotational symmetry. The rotor shown in Fig. 1(e) has a rotational frequency of ω. The distance between the origami drivers and the rotor is defined as "gap," which is commonly different from 0.34 nm and can affect the rotor's stable rotational frequency (SRF).

B. Mechanism of the RGORI driver

In this study, we use the RGORI to actuate the rotation of the rotor in Figs. 1(d)–1(e). Before verifying the feasibility of the nanomotor, we demonstrate the driving mechanism of the model. It is known that the atoms in both the rotor and the drivers have thermal vibration at finite temperature. When gap < 1.0 nm, the RGORI drivers and the rotor have apparent nonbonding interaction, and thermal vibration leads to a collision between the drivers and the rotor. Once the drivers' repulsive force causes unidirectional moment to the rotor, the torque moment will accelerate the rotor to rotate [29,38]. Further, it is necessary to show evidence that indicates the rotationally symmetric layout of the four drivers can provide unidirectional moment on the rotor.

In Fig. 2, six snapshots of the RGORI driver relaxing indicate that the bond structure at the tip is asymmetric (see the upper layer of Fig. 2), which is essential for the unidirectional repulsion from the tip to the rotor. The tip of origami mainly vibrates in the x direction. For showing the dynamic properties of the origami, the curves of the mass center of a tip versus time are plotted for temperatures of 100 and 300 K, and the frequencies together with the corresponding amplitudes are obtained via FFT [39] (Fig. 3). At lower temperature, the tip has higher frequency due to higher stiffness but a lower amplitude because of weaker thermal vibration. The vibration amplitude of the tip determines the magnitude of repulsive force to the rotor.

C. Methodology

The molecular-dynamics simulation approach is adopted to investigate the dynamic response of the rotor at finite temperature. The molecular-dynamics simulations are conducted on the open-source code LAMMPS [40]. The interaction among atoms is evaluated by the adaptive intermolecular reactive empirical bond order (AIREBO) potential [41], which can describe both bonding and nonbonding interactions [42].

For each simulation, the following essential steps are required:

Step (1). Build a nanomotor model with specific geometry factors such as α and ω.

Step (2). Reshape the geometry of the stator and rotors by minimizing the potential energy of the system.

Step (3). Fix the atoms in the stators and fix the legs of the drivers.

Step (4). Relax the system in a canonical ensemble with a given temperature between 8 and 300 K. The temperature is controlled by the Nosé-Hoover thermostat [43,44].

Step (5). Record ω of the rotor for 20 ns. The time step is 0.001 ps.

The system's state is monitored via the observation of the variation of potential energy (VPE) of the system. The value of V_{PE} is the difference between the current and the initial potential of the system, i.e.,

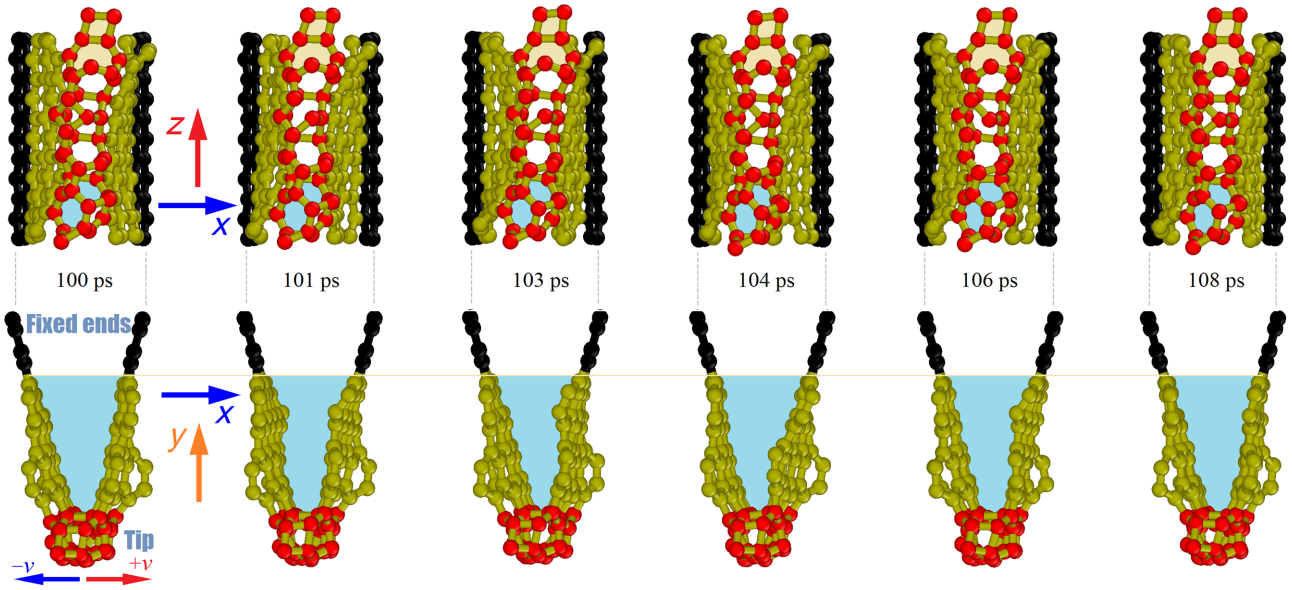

FIG. 2. Snapshots of the RGORI driver with $\alpha = 30°$ being relaxed at 300 K. Vibration of tip can be illustrated by variation of the driver's configuration.

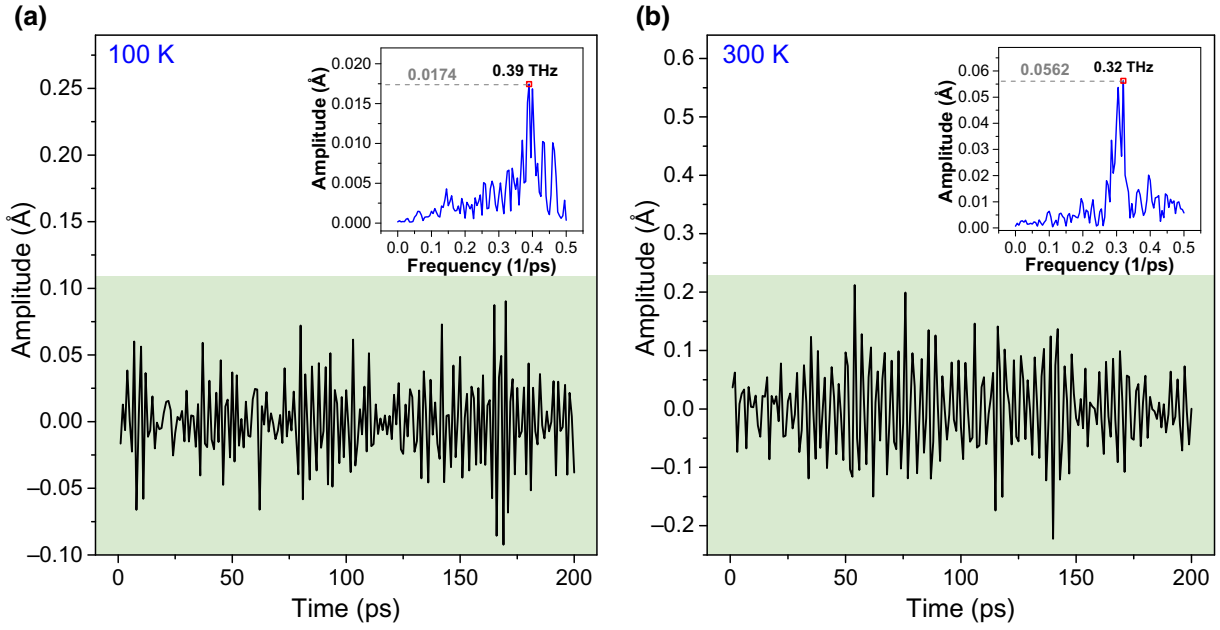

FIG. 3. Time history of thermal vibration of the mass center of the driver's tip at different temperatures. The driver is made from the RGORI with $\alpha = 30°$ in relaxation (a) at 100 K, (b) at 300 K. Insets are FFT results, with peak amplitude at 0.39 THz for 100 K, and at 0.32 THz for 300 K.

$$V_{\mathrm{PE}}(t) = P(t) - P(t_0), \tag{1}$$

where $P(t)$ and $P(t_0)$ are the total potential energy of the system at time t and t_0, respectively. They can be determined by the AIREBO potential function.

D. Stable rotational frequency of the rotor

At finite temperature, the atoms that are not fixed have thermal vibration, described as phonons propagating in the system. When the RGORI drivers press the rotor, the thermal vibration of atoms on the components will enhance their interaction. Briefly, the collision between the rotor and the drivers happens drastically. In collision, the repulsion from the drivers will drive the rotor to rotate in unidirection and the frequency ω is given as

$$\omega(t) = \int_{s=0}^{t} \varepsilon(s)ds = \int_{s=0}^{t} \frac{1}{J_z}(M_{\mathrm{driver}} - M_{\mathrm{stator}})ds, \tag{2}$$

where $\varepsilon(t)$ is the rotor's transiently angular acceleration and J_z the mass inertia of the rotor about its rotational axis (i.e., z axis). M_{driver} is the driving moment from the origami drivers, and M_{stator} is the friction-induced resistant moment from the two stators [45,46]. Since M_{stator} increases with the increase of ω, ω must converge to a maximal value, with which the rotor is in a stable rotational state. The maximal value of ω is known as SRF.

III. RESULTS AND DISCUSSION

A. Effect of origami angle (α)

From Fig. 1(a), we know that, even when relaxed at the same temperature, the configuration of the origami's tip is different if the origami has a different angle. For showing the feasibility that the tip can drive the rotor to rotate, here, four angles in each type of driver are considered in the nanomotor system. Figure 4 gives the historical curves of the rotor's rotational frequency (ω) corresponding to each of the four origami angles. In the four cases, the values of gap, i.e., the distance between the drivers' tips and the rotor, are identical to 0.34 nm. Meanwhile, the nanomotors are relaxed at 100 K.

Figure 4 indicates that the RGORI drivers corresponding to $\alpha = 20°$ and 30° cannot drive the rotor to rotate since the curves slightly fluctuate near zero, i.e., within the mean value of SRF $= -2.6$ GHz and 0, respectively. It means that the two types of drivers provide weak repulsion to the rotor. According to the configurations of the two types of drivers shown in Fig. 1(c), some of the tip atoms in the RGORI driver corresponding to $\alpha = 20°$ do not connect the rest tips' atoms. Hence the tip atoms provide weak repulsion to the rotor. For the drivers corresponding to $\alpha = 30°$, it shrinks after relaxation [this can be verified by comparing the sizes of the four relaxed drivers in Fig. 1(c).]. When the distance between the rotor and the drivers' fixed ends is constant, the tips of the drivers corresponding to $\alpha = 30°$ provide very weak repulsion to the rotor during the thermal vibration-induced collision. In the two remaining models

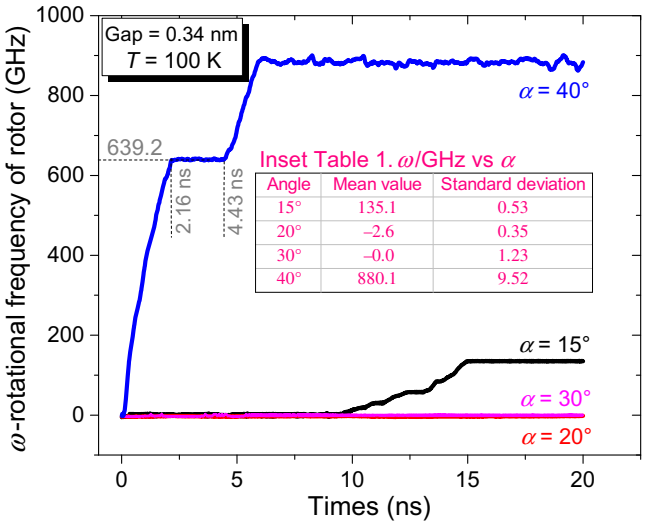

Angle	Mean value	Standard deviation
15°	135.1	0.53
20°	–2.6	0.35
30°	–0.0	1.23
40°	880.1	9.52

FIG. 4. Evolution history of the rotational frequency of the rotor when driven by the origami with different initial angles. Gap = 0.34 nm; $T = 100$ K.

with $\alpha = 15°$ and 40°, the rotor is successfully actuated to rotate with SRF at the level between 100 and 1000 GHz. Hence, we conclude that the graphene origami can act as a driver in a nanomotor at certain values of angles α.

In Fig. 4, we also find that each of the two curves of ω contain a stair before approaching SRF. They locate in approximately 135.1 GHz at $\alpha = 15°$ and approximately 880.1 GHz at $\alpha = 40°$. The stair duration could be over 2 ns (see the blue curve in Fig. 4). Actually, the platform indicates that the rotor is in an equilibrium state during rotation. The equilibrium state is determined by the active force from the drivers and the frictional forces from the stators. On the nanoscale, the intershell friction between neighboring carbon nanotubes is sensitive to the relative sliding speed (or rotational frequency) and their interface [45,46]. The stair in the ω curve indicates that both the active force from the drivers and the frictional force increase simultaneously [see Eq. (2)]. When the driving force increases further while the frictional force approaches the local maximum, the rotor is accelerated again, e.g., the blue curve jumps after 4.43 ns, till ω approaches SRF.

B. Effect of "gap"

In the above discussion, the values of gap in the four models are equal to 0.34 nm. Gap is the other essential factor that influences the interaction between the drivers and the rotor. For example, the repulsion on the rotor becomes stronger when gap is lower. To evaluate the effect of gap on the rotational frequency of the rotor, herein, the nanomotor with the origami angle $\alpha = 15°$ at 100 K is involved in the discussion.

Figure 5(a) provides curves of ω corresponding to five different gaps. The maximal stable value of ω increases mainly with decreasing of the gap. For example, SRF will reach 365.8 GHz when gap decreases to 0.32 nm. At gap = 0.28 nm, SRF is higher than 1000 GHz. However, when gap decreases further, e.g., to 0.26 nm, the value of SRF is only 377.6 GHz, which is much less than that at gap = 0.28 nm. The reason is that the repulsive force between the tips of drivers and the rotor becomes stronger at a lower value of gap. When gap = 0.26 nm, the repulsion is so strong that the drivers are forced to have large deformation, which leads to displacement of the tips from their original positions. Therefore, the tips can only provide lower effective driving force to the rotor.

Meanwhile, in the black curve (gap = 0.26 nm), there are several steps before ω approaches SRF. This phenomenon reveals the interaction between the drivers and

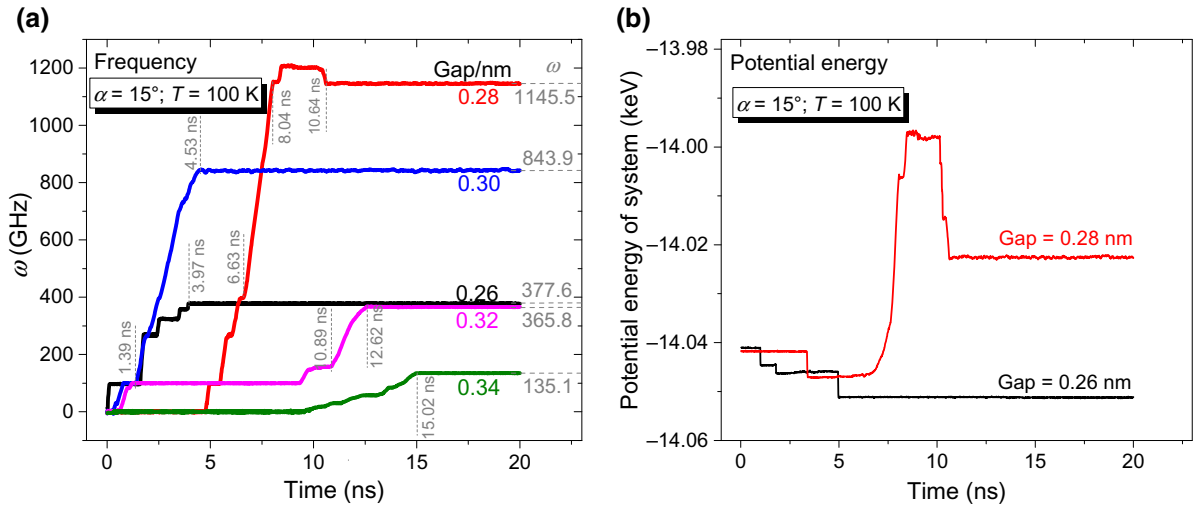

FIG. 5. Dynamic response of the rotor when driven at 100 K by the RGORI with $\alpha = 15°$ using different gaps. (a) Rotational frequency; (b) potential energy of the system.

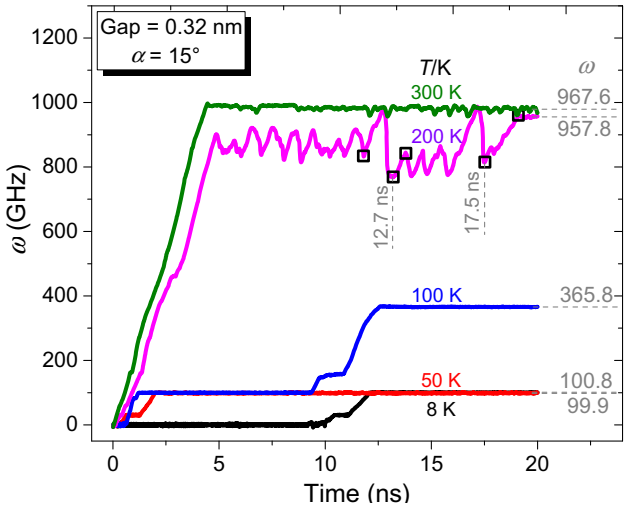

FIG. 6. Evolution history of the rotational frequency of the rotor when driven by the origami with $\alpha = 15°$ and gap = 0.32 nm at different temperatures.

the rotor changes gradually and reflects the gradual deformation of drivers from another viewpoint. It can be verified by the steep changes of the system's potential energy [Fig. 5(b)]. Considering the two facts, i.e., over 1000 GHz at gap = 0.28 nm and strong repulsion at gap = 0.26 nm, the value of gap is recommended to be between 0.30 and 0.34 nm in a rotary nanomotor with stable rotation.

On another aspect of the acceleration of the rotor, $\varepsilon(t)$ needs to be described as well. The slope of the ω curve can illustrate the acceleration of the rotor. Figure 5 shows that the slopes of the curves at the jump stages are higher at a lower value of gap. For example, when gap = 0.34 nm, ω increases from zero to SRF (i.e., with increment of 135.1 GHz) during approximately 5 ns, with a slope of approximately 27.2 GHz/ns. When gap = 0.28 nm, ω jumps up from approximately 400 GHz at 6.63 ns to approximately 1150 GHz at 8.04 ns, and the slope is approximately 531.9 GHz/ns. According to the formula that $\varepsilon(t) = (M_{\text{driver}} - M_{\text{stator}})/J_z$, we know that the drivers must provide a stronger moment onto the rotor if the rotor has higher acceleration and constant moment inertia. Hence, a lower distance between the rotor and the drivers will introduce both higher acceleration and higher SRF of the rotor.

C. Effect of temperature

Since the drivers are working at finite temperature, their tips' thermal vibration induces a driving force that can actuate the rotor to rotate. Hence, the temperature of the system must affect the rotation of the rotor. Figure 6 shows that the rotational frequencies of the rotor excited by the drivers with $\alpha = 15°$ and gap = 0.32 nm are collected at a temperature between 8 and 300 K.

When observing the curve relating to 200 K in Fig. 6, one can find that ω fluctuates drastically after approximately 4 ns of acceleration. We pick up five representative snapshots of the system at a different time between 11 and 20 ns (Fig. 7). At each snapshot, the rotor has large transversal deformation during rotating. As we know, rotating at too high speed, e.g., approximately 800 GHz (pink line), the deformed rotor is under strong eccentric force. In rotating, the distance between the rotor and the drivers changes periodically. Hence, the drivers irregularly vibrate when impacted by the rotor periodically besides thermal vibration. It means that the interaction between the rotor and the drivers is not stable, which leads to fluctuation of ω. After 19 ns, ω becomes stable and approaches SRF, i.e., 957.8 GHz.

IV. CONCLUSIONS

In this study, to drive a CNT to rotate, we introduce GORI into the nanomotor model as drivers. For verifying the feasibility of the nanomotor model, the driving mechanism of the GORI drivers is revealed, and the molecular-dynamics simulations are used to show the effects of geometry and temperature on the rotation of

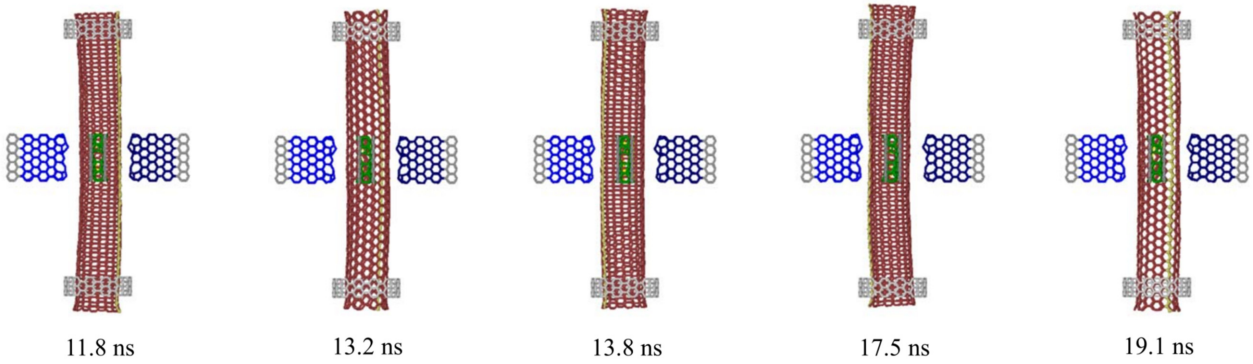

FIG. 7. Five snapshots of the system with $\alpha = 15°$ and gap = 0.32 nm at 200 K.

rotor. Conclusions are drawn for manufacturing a rotary nanomotor based on the present model.

First, for a cantilevered GORI, the unfixed atoms have thermal vibration, e.g., excited by a laser, which leads to vibration of the GORIs tip. When several drivers from RGORI are laid in rotational symmetry around a CNT rotor, their tips will induce torque moment and be applied to the CNT rotor. Accelerated by the torque moment, the rotor has a SRF when the resistant torque moment from stators can balance the driving moment.

Second, the atoms in both the rotor and the drivers have thermal vibration at finite temperature. When gap, the distance between the rotor and the tips of RGORI, is less than 1.0 nm, the RGORI drivers and the rotor have obvious nonbonding interaction. At a lower temperature, the tips have higher frequency due to higher stiffness, but have lower amplitudes because of weaker thermal vibration. The vibration amplitude of the tip determines the magnitude of repulsive force to the rotor. Hence, the value of SRF of CNT rotor mainly increases with decreasing of gap. An interval of [0.3 nm, 0.34 nm] is recommended for gap in the design of the nanomotor.

Third, the temperature is another factor affecting SRF, i.e., stronger thermal vibration of the tips will produce larger driving forces onto the rotor and leads to a higher value of SRF.

In the present study, the proposed model for rotary nanomotor is verified by molecular-dynamics simulations only. Experimental implementation is expected in the near future. A challenge is the assembly of the RGORI drivers around the CNT rotor because the extremely high precision of their locations is required at such a strong nonbonding interaction environment.

The potential application of the nanomotor is as an engine in a nanomachine. For the simplest nanomachine, it should contain three components, e.g., a nanomotor, a frame, and a functional component. Both nanomotor and the functional component should be assembled on the frame. The present intricate nanosystem will be studied in the future.

ACKNOWLEDGMENTS

We acknowledge the financial support from the National Natural Science Foundation of China (Grant No. 11772204), National Key Research and Development Plan, China (Grant No. 2017YFC0405102), and State Key Laboratory of Structural Analysis for Industrial Equipment, Dalian University of Technology, Dalian 116024, China (Grant No. GZ18111).

[1] Press release: The Nobel Prize in Chemistry 2016. Available from: http://www.nobelprize.org/nobel_prizes/chemistry/laureates/2016/press.html, 2016 (Accessed 2 January 2021).

[2] K. S. Novoselov, A. K. Geim, S. V. Morozov, D. Jiang, Y. Zhang, S. V. Dubonos, I. V. Grigorieva, and A. A. Firsov, Electric field effect in atomically thin carbon films, Science **306**, 666 (2004).

[3] S. Iijima, Helical microtubules of graphitic carbon, Nature **354**, 5658 (1991).

[4] C. Lee, X. Wei, J. W. Kysar, and J. Hone, Measurement of the elastic properties and intrinsic strength of monolayer graphene, Science **321**, 385 (2008).

[5] Q. Pei, Y. Zhang, and V. Shenoy, A molecular dynamics study of the mechanical properties of hydrogen functionalized graphene, Carbon **48**, 898 (2010).

[6] M.-F. Yu, O. Lourie, M. J. Dyer, K. Moloni, T. F. Kelly, and R. S. Ruoff, Strength and breaking mechanism of multiwalled carbon nanotubes under tensile load, Science **287**, 637 (2000).

[7] Z. Qin, Q.-H. Qin, and X.-Q. Feng, Mechanical property of carbon nanotubes with intramolecular junctions: Molecular dynamics simulations, Phys. Lett. A **372**, 6661 (2008).

[8] J. Cumings and A. Zettl, Low-friction nanoscale linear bearing realized from multiwall carbon nanotubes, Science **289**, 602 (2000).

[9] R. Zhang, Z. Ning, Y. Zhang, Q. Zheng, Q. Chen, H. Xie, Q. Zhang, W. Qian, and F. Wei, Superlubricity in centimetres-long double-walled carbon nanotubes under ambient conditions, Nat. Nanotech. **8**, 912 (2013).

[10] E. H. Cook, M. J. Buehler, and Z. S. Spakovszky, Mechanism of friction in rotating carbon nanotube bearings, J. Mech. Phys. Solids **61**, 652 (2013).

[11] S. Zhang, W. K. Liu, and R. S. Ruoff, Atomistic simulations of double-walled carbon nanotubes (DWCNTs) as rotational bearings, Nano Lett. **4**, 293 (2004).

[12] K. Cai, H. Yin, Q.-H. Qin, and Y. Li, Self-excited oscillation of rotating double-walled carbon nanotubes, Nano Lett. **14**, 2558 (2014).

[13] A. Fennimore, T. Yuzvinsky, W.-Q. Han, M. Fuhrer, J. Cumings, and A. Zettl, Rotational actuators based on carbon nanotubes, Nature **424**, 408 (2003).

[14] A. Barreiro, R. Rurali, E. R. Hernández, J. Moser, T. Pichler, L. Forro, and A. Bachtold, Subnanometer motion of cargoes driven by thermal gradients along carbon nanotubes, Science **320**, 775 (2008).

[15] B. Wang, L. Vuković, and P. Král, Nanoscale Rotary Motors Driven by Electron Tunneling, Phys. Rev. Lett. **101**, 186808 (2008).

[16] W. Qiu, Q. Li, Z.-K. Lei, Q.-H. Qin, W.-L. Deng, and Y.-L. Kang, The Use of a carbon nanotube sensor for measuring strain by micro-Raman spectroscopy, Carbon **53**, 161 (2013).

[17] R. G. Knobel, Weighing single atoms with a nanotube, Nat. Nanotech. **3**, 525 (2008).

[18] L. Yang, K. Cai, J. Shi, Y. M. Xie, and Q.-H. Qin, Nonlinear dynamic behavior of a clamped–clamped beam from BNC nanotube impacted by fullerene, nonlin, Nonlinear Dyn. **96**, 1133 (2019).

[19] M. K. Blees, A. W. Barnard, P. A. Rose, S. P. Roberts, K. L. McGill, P. Y. Huang, A. R. Ruyack, J. W. Kevek, B.

Kobrin, and D. A. Muller, Graphene kirigami, Nature **524**, 204 (2015).
[20] K. Cai, X. Li, J. Shi, and Q.-H. Qin, Nanospring from partly hydrogenated graphene ribbon: A molecular dynamics study, Appl. Surf. Sci. **541**, 148507 (2020).
[21] P. Král and H. Sadeghpour, Laser spinning of nanotubes: A path to fast-rotating microdevices, Phys. Rev. B **65**, 161401 (2002).
[22] D. Srivastava, A phenomenological model of the rotation dynamics of carbon nanotube gears with laser electric fields, Nanotechnology **8**, 186 (1997).
[23] R. E. Tuzun, D. W. Noid, and B. G. Sumpter, Dynamics of a laser driven molecular motor, Nanotechnology **6**, 52 (1995).
[24] J. Ahn, Z. Xu, J. Bang, Y.-H. Deng, T. M. Hoang, Q. Han, R.-M. Ma, and T. Li, Optically Levitated Nanodumbbell Torsion Balance and GHz Nanomechanical Rotor, Phys. Rev. Lett. **121**, 033603 (2018).
[25] J. W. Kang and H. J. Hwang, Nanoscale carbon nanotube motor schematics and simulations for micro-electro-mechanical machines, Nanotechnology **15**, 1633 (2004).
[26] A. Prokop, J. Vacek, and J. Michl, Friction in carborane-based molecular rotors driven by gas flow or electric field: Classical molecular dynamics, ACS Nano **6**, 1901 (2012).
[27] R.-Y. Dong and B.-Y. Cao, Superhigh-speed unidirectional rotation of a carbon nanotube in a sheared fluid and its decoupled dynamics, RSC Adv. **5**, 88719 (2015).
[28] K. Cai, Y. Li, Q.-H. Qin, and H. Yin, Gradientless temperature-driven rotating motor from a double-walled carbon nanotube, Nanotechnology **25**, 505701 (2014).
[29] K. Cai, J. Yu, J. Shi, and Q.-H. Qin, Spectrum of temperature-dependent rotational frequency of the rotor in a thermally driven rotary nanomotor, J. Phys. Chem. C **121**, 16985 (2017).
[30] L. Yang, K. Cai, J. Shi, and Q.-H. Qin, Significance tests on the output power of a thermally driven rotary nanomotor, Nanotechnology **28**, 215705 (2017).
[31] K. Cai, J. Yu, J. Shi, and Q.-H. Qin, A method for measuring rotation of a thermal carbon nanomotor using centrifugal effect, Sci. Rep. **6**, 27338 (2016).
[32] Y. Li, A. Wang, and J. Shi, Gap effect on stable rotation of a carbon nanotube nearby diamond needles, Computat. Mater. Sci. **156**, 260 (2019).
[33] J. Shi, A. Wang, B. Song, and K. Cai, A GHz rotary nanoflake driven by diamond needles: A molecular dynamics study, Mater. Des. **191**, 108593 (2020).
[34] X. Lin and Q. Han, Molecular dynamic simulation of defect-driven rotary system based on a triple-walled carbon nanotube and graphene, Molecu. Simula. **46**, 356 (2020).
[35] J. Mu, C. Hou, H. Wang, Y. Li, Q. Zhang, and M. Zhu, Origami-inspired active graphene-based paper for programmable instant self-folding walking devices, Sci. Adv. **1**, e1500533 (2015).
[36] H. Chen, X.-L. Zhang, Y.-Y. Zhang, D. Wang, D.-L. Bao, Y. Que, W. Xiao, S. Du, M. Ouyang, S. T. Pantelides, and Atomically Precise, Custom-design origami graphene nanostructures, Science **365**, 1036 (2019).
[37] D. T. Ho, H. S. Park, S. Y. Kim, and U. Schwingenschlögl, Graphene origami with highly tunable coefficient of thermal expansion, ACS Nano **14**, 8969 (2020).
[38] K. Cai, J. Wan, Q.-H. Qin, and J. Shi, Quantitative control of a rotary carbon nanotube motor under temperature stimulus, Nanotechnology **27**, 055706 (2016).
[39] M. J. Mohlenkamp, A fast transform for spherical harmonics, J. Fourier Analy. Appl. **5**, 159 (1999).
[40] S. Plimpton, Fast parallel algorithms for short-range molecular dynamics, J. Comput. Phys. **117**, 1 (1995).
[41] S. J. Stuart, A. B. Tutein, and J. A. Harrison, A reactive potential for hydrocarbons with intermolecular interactions, J. Chem. Phys. **112**, 6472 (2000).
[42] J. E. Jones, On the determination of molecular fields.—II. From the equation of state of a Gas, Proc. R. Soc. Lond., A 106, 463 (1924).
[43] S. Nosé, A unified formulation of the constant temperature molecular dynamics methods, J. Chem. Phys. **81**, 511 (1984).
[44] W. G. Hoover, Canonical dynamics: Equilibrium phase-space distributions, Phys. Rev. A **31**, 1695 (1985).
[45] W. Guo, Y. Guo, H. Gao, Q. Zheng, and W. Zhong, Energy Dissipation in Gigahertz Oscillators From Multiwalled Carbon Nanotubes, Phys. Rev. Lett. **91**, 125501 (2003).
[46] J. Servantie and P. Gaspard, Translational dynamics and friction in double-walled carbon nanotubes, Phys. Rev. B **73**, 125428 (2006).